Journal of Materials Chemistry C

ROYAL SOCIETY OF CHEMISTRY

PAPER

Published on 29 June 2026
Licence and permissions

Check for updates

Cite this: DOI: 10.1039/d6tc00909c

A design strategy for inducing delayed fluorescence *via* molecular flexibility: structure–property relationships in organic emitters

Gyana Prakash Nanda,[a] Suvendu Dey,[a] Bahadur Sk,[a] Rajan Suraksha,[a] Sanyam,[b] Anirban Mondal*[b] and Pachaiyappan Rajamalli*[a]

Received 21st March 2026,
Accepted 25th June 2026

DOI: 10.1039/d6tc00909c

rsc.li/materials-c

Modification of the molecular structure can drastically change the photophysical properties of luminogens; establishing these structure–property relationships provides a roadmap for the rational design of novel materials. In this study, we analyzed the detailed structure–property relationships of our synthesized emitters with those of previously reported compounds. **BP-Cz**, with a benzophenone acceptor linked to carbazole, is a well-known phosphorescent emitter with an excited state lifetime of 518 ms. By inserting a nitrogen atom into the acceptor moiety, the emitter **4BPy-Cz** was reported to be a non-TADF and non-phosphorescent compound. Insertion of nitrogen into the molecular structure stabilized the excited states, resulting in a red shift in the absorption and emission spectra of **4BPy-Cz**. The donor was made flexible and **4BPy-PTA** was synthesized using *N*,*N*-ditolyl amine as the donor, which started showing TADF properties. The fabricated OLED exhibited an EQE_{max} of 6.4%, exceeding the theoretical limit for fluorescent OLEDs and 1.5 times higher than that of the **4BPy-Cz** device. To investigate the effect of peripheral groups, two additional emitters, **4BPy-PBPA** and **4BPy-PMPA**, bearing *N*,*N*-di-*tert*-butylphenyl amine and *N*,*N*-dimethoxyphenyl amine donors, respectively, were synthesized. Surprisingly, the EQE_{max} values for **4BPy-PBPA** and **4BPy-PMPA** increased to 17.3% and 16.2%, respectively. Theoretical studies suggested the active involvement of the upper triplet state in the rISC process. Temperature-dependent photophysical studies and kinetic parameters confirm the TADF behavior of all three emitters. This study demonstrates the reappearance of delayed fluorescence properties in the system after inducing molecular flexibility.

1. Introduction

Structure–property relationships play a pivotal role in governing the photophysical and optoelectronic behaviors of organic emitters, providing a fundamental framework for the rational design of high-performance luminescent materials.[1–5] Subtle modifications in the molecular structure such as donor–acceptor architecture, conjugation length, molecular rigidity or flexibility, and substitution pattern can significantly influence key photophysical properties including emission wavelength, full width at half maximum (FWHM), singlet–triplet energy splitting (ΔE_{ST}), radiative and non-radiative decay pathways, and charge-transport characteristics.[4,6–8] In particular, tailoring molecular conformation and flexibility offers an effective strategy to modulate excited-state dynamics by controlling intramolecular charge transfer and spin-related processes.[9,10] Through deliberate structural engineering, it is possible to fine-tune emission colour, enhance exciton utilization, and induce delayed fluorescence, highlighting the critical importance of structure–property correlations in the development of next-generation organic light-emitting materials.

Here, we have designed three organic luminescent materials, namely **4BPy-PTA**, **4BPy-PBPA**, and **4BPy-PMPA**. Structurally, **4BPy-PTA** is the flexible form of a reported non-DF emitter, **4BPy-Cz**, while **4BPy-PBPA** is another flexible counterpart of a known TADF emitter, 4BPy-tCz (Fig. 1a).[11,12] All three emitters show substantial PLQYs above 90% under CBP-doped conditions and exhibit a faster fluorescence radiative rate (k_pR) in the order of 10^8 s^{-1}. These emitters show long delayed fluorescence lifetime (τ_{avg}) values of 0.86 ms in **4BPy-PTA**, 3.07 ms in **4BPy-PBPA**, and 0.52 ms in **4BPy-PMPA**. Theoretical studies and spin–orbit coupling (SOC) calculations indicate the involvement of the upper triplet state (T_2) in the exciton upconversion process. The vacuum-deposited OLED devices of **4BPy-PTA**, **4BPy-PBPA**,

[a] *Materials Research Centre, Indian Institute of Science (IISc), Bangalore, 560012, India. E-mail: rajamalli@iisc.ac.in, gyanananda@iisc.ac.in, suvendudey@iisc.ac.in, bahadursk@hotmail.com, surakshar@iisc.ac.in*

[b] *Department of Chemistry, Indian Institute of Technology Gandhinagar, Palaj, Gandhinagar, 382355, Gujarat, India. E-mail: amondal@iitgn.ac.in, sanyamsanyam@iitgn.ac.in*

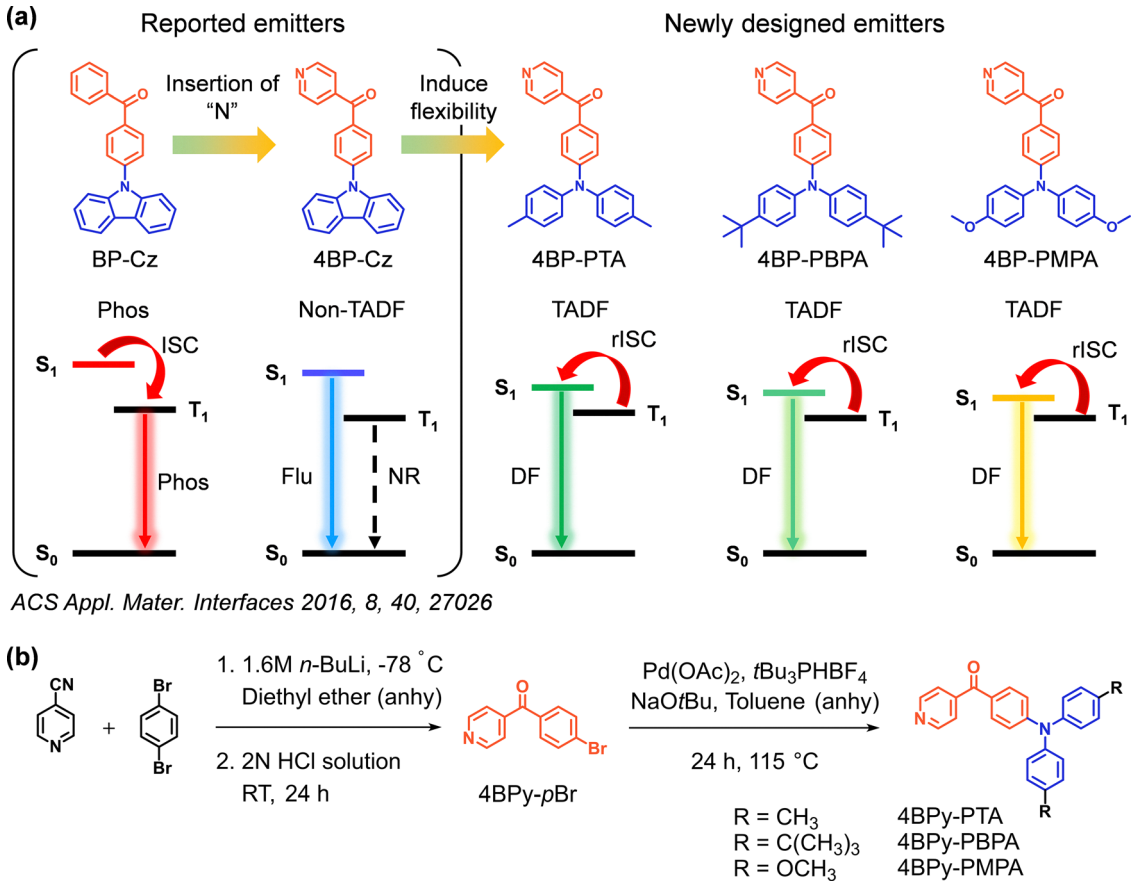

Fig. 1 (a) Molecular design strategy; (b) synthesis scheme of the emitters.

and **4BPy-PMPA** showed EQE_{max} values of 6.5, 17.3, and 16.2%, respectively. Better EL performance in **4BPy-PBPA** and **4BPy-PMPA** devices was possible due to more efficient vibronic coupling between triplet states than in **4BPy-PTA**. Interestingly, all the flexible emitters showed higher external quantum efficiencies than their reported rigid counterparts. This study highlights the importance of molecular flexibility in an emitter for regaining delayed fluorescence.

2. Design strategy

2.1. Molecular structure and synthesis

(4-(9*H*-Carbazol-9-yl)phenyl)(phenyl)methanone (**BP-Cz**), having a benzophenone acceptor linked to carbazole, is a well-known phosphorescent emitter exhibiting an excited state lifetime of 518 ms.[11] By changing the acceptor unit from benzophenone to benzoyl pyridine, the emitter **4BPy-Cz** was reported to be a non-TADF and non-phosphorescent compound (Fig. 1a).[12] Here, the insertion of a nitrogen atom converts the $T_1 \rightarrow S_0$ transition into a non-radiative one. Furthermore, the nitrogen atom in the acceptor unit stabilized the excited states, resulting in red shifts in the absorption and emission spectra of **4BPy-Cz**.[8] Here, we extended the study by replacing the rigid carbazole donor in **4BPy-Cz** with flexible diaryl amine units. Three organic emitters, namely (4-(di-*p*-tolylamino)phenyl)(pyridin-4-yl)methanone (**4BPy-PTA**), (4-(bis(4-(*tert*-butyl)phenyl)amino)phenyl)(pyridin-4-yl)methanone (**4BPy-PBPA**), and (4-(bis(4-methoxyphenyl)amino)phenyl)-(pyridin-4-yl)methanone (**4BPy-PMPA**), were synthesized using the reported procedure.[13,14] All three emitters contain a similar 4-benzoylpyridine (4BPy) acceptor unit and carry different flexible donor groups of di-*p*-tolylamine, di-*tert*-butyl-phenylamine, and bis(4-methoxyphenyl)amine, which were coupled *via* a Buchwald–Hartwig amination reaction (Fig. 1b).[13,14] The detailed synthesis procedure and structural characterization of the emitters are provided in the SI.

The molecular structures of the emitters **4BPy-PTA** and **4BPy-PBPA** were also confirmed through single-crystal XRD analysis. Single crystals of **4BPy-PTA** and **4BPy-PBPA** with a monoclinic unit cell were prepared (Tables S1 and S2). However, despite repeated attempts, crystals of sufficient quality for structural determination could not be obtained for **4BPy-PMPA**. According to a previous report, the phenyl rings of the 9*H*-carbazole group remain coplanar,[12] but in this case the aryl units in the di-*p*-tolylamine/PTA, bis(4-(*tert*-butyl)phenyl)amine/PBPA, and bis(4-methoxyphenyl)amine/PMPA donors exhibited significant bond twisting (Fig. S1 and S2). The twisting angles of the three phenyl rings attached to the central nitrogen atom were measured to be 56.58° (C10–N2–C13–C14) and 79.25° (C10–N2–C19–C20) relative to the bridging phenyl ring of the acceptor core for **4BPy-PTA**, while the values were 49.05° (C10–N1–C13–C18) and 76.35°

Table 1 Photophysical properties of **4BPy-PTA**, **4BPy-PBPA**, and **4BPy-PMPA**

Emitter	λ_{abs}[a] (nm)	λ_{em}[b] (nm)	S_1/T_1[c] (eV)	ΔE_{ST}[d] (eV)	λ_{em}[e] (nm)	ΔE_{ST}[f] (eV)	HOMO/LUMO[g] (eV)	PLQY[h] air/N_2 (%)	T_d[i] (°C)
4BPy-PTA	378	501	2.79/2.61	0.18	500	0.32	−5.38/−2.49	82.4/92.0	325
4BPy-PBPA	380	514	2.75/2.61	0.14	505	0.28	−5.38/−2.49	91.2/100	322
4BPy-PMPA	379	542	2.62/2.62	≈0.00	531	0.22	−5.22/−2.39	71.4/93.0	342

[a] Absorption maxima of the emitters in 0.01 mM toluene solution. [b] Emission maxima of the emitters in toluene solution. [c] Singlet and triplet energy levels of the emitters in toluene solution. [d] Singlet–triplet energy gaps of the emitters in toluene. [e] Emission maxima of the emitters in the 7 wt% emitter:CBP host doped film. [f] Singlet–triplet energy gaps of the emitters in the CBP doped film. [g] HOMO and LUMO energy levels obtained from CV. [h] Photoluminescence quantum yield of the emitter in the CBP doped film measured under air and inert conditions. [i] Decomposition temperature of the emitters.

(C10–N1–C19–C24) in the case of **4BPy-PBPA**. This signifies a highly twisted, non-planar conformation as compared to the fused phenyl rings of the 9*H*-carbazole group, thereby imparting enhanced molecular flexibility. The dihedral angles (or torsion angles) of the emitters are provided in the SI (Fig. S1 and S2).

2.2. Thermal and electrochemical properties

To obtain ultrapure materials, the emitters were purified using the temperature-gradient vacuum sublimation technique. The thermal stability of the emitters was assessed by thermogravimetric analysis (TGA) under a nitrogen atmosphere (Fig. S3). Among the three emitters, **4BPy-PMPA** showed the highest thermal stability, with a degradation temperature (T_d) of 342 °C, followed by **4BPy-PTA** and **4BPy-PBPA** (Table 1). The highest occupied molecular orbital (HOMO) and lowest unoccupied molecular orbital (LUMO) energy levels were calculated by cyclic voltammetry analysis using a 1 mM solution of the compound prepared in a degassed dichloromethane solvent. The detailed procedure is described in the SI (Fig. S4). **4BPy-PTA** and **4BPy-PBPA** possess similar HOMO and LUMO energy levels of −5.38 eV and −2.49 eV, respectively. On the other hand, **4BPy-PMPA** shows comparatively shallower HOMO (−5.22 eV) and LUMO (−2.39 eV) energy levels due to the strong electron-donating ability of PMPA (Table 1).

3. Results and discussion

3.1. Photophysical properties

3.1.1. Steady-state PL measurements. UV–visible absorption spectra of the emitters were recorded in solution at 0.01 mM concentration (Fig. 2a), and the corresponding results are summarized in Table 1. Toluene solutions of all three emitters showed broad absorption bands with peak maxima at 379 nm, corresponding to an intramolecular charge-transfer (ICT) transition. The identical absorption maxima of the emitters suggest the negligible impact of the peripheral groups on the ground state electronic structure. From the onsets of the absorption spectra, the optical bandgaps (E_g) were evaluated. Both **4BPy-PTA** and **4BPy-PBPA** showed a similar E_g of 2.88 eV, whereas in **4BPy-PMPA**, the energy gap was slightly reduced to 2.82 eV. The reduced bandgap in **4BPy-PMPA** is due to the strong electron-donating ability of the methoxyphenyl amine group, which is in accordance with the electrochemical results.

The photoluminescence (PL) properties of the emitters were investigated in both solution (0.01 mM) and under 4,4′-bis(*N*-carbazolyl)-1,1′-biphenyl (CBP) host-doped conditions. The solution PL was recorded at an excitation wavelength of 380 nm (Fig. 2a and b). The toluene solutions of **4BPy-PTA** and **4BPy-PBPA** showed intense green emission with emission maxima (PL_{max}) at 501 and 514 nm, respectively. This 13 nm redshift in **4BPy-PBPA** was due to the increased electron-donating ability of the tertiary butyl than the methyl group. On the other hand, **4BPy-PMPA** shows emission in the lower energy region, with a PL_{max} at 542 nm and a larger full width at half-maximum (FWHM) than the other two emitters. The comparatively larger Stokes shift and broader FWHM in **4BPy-PMPA** indicate a greater extent of structural relaxation in the excited state of the emitter, which is due to the strong electron-donating ability of the methoxy peripheral group, resulting in charge-transfer (CT) dominated excited states (Fig. 2a).[15] Phosphorescence spectra of the emitters were recorded at low temperature (77 K), which showed their partial locally excited (LE) character (Fig. 2b). From the onset of fluorescence and phosphorescence spectra, singlet (S_1) and triplet (T_1) excited state energy levels and their singlet–triplet energy difference (ΔE_{ST}) were calculated (Table 1). The toluene solution of **4BPy-PTA** shows the highest ΔE_{ST} of 0.18 eV among the three emitters, whereas **4BPy-PMPA** shows the lowest ΔE_{ST} of 0.003 eV. Compared to the rigid counterpart (**4BPy-Cz**/0.29 eV), ΔE_{ST} has reduced in the flexible emitter (**4BPy-PTA**). The ΔE_{ST} values obtained for the emitters are sufficiently lower than the minimum energy barrier required for triplet exciton upconversion; hence, rISC can be expected in these flexible systems.[8,16–18]

Fluorescence spectra of the emitters showed broad, structureless emission, suggesting their CT nature, which was confirmed through solvatochromic studies (Fig. 2c–e).[19] In the non-polar *n*-hexane solvent, **4BPy-PTA**, **4BPy-PBPA**, and **4BPy-PMPA** showed emissions with PL_{max} at 447, 448, and 486 nm, respectively. With increasing solvent polarity, the emission color started red shifting, followed by a reduction in emission intensity and broadening of the emission spectra. In chloroform, **4BPy-PTA** and **4BPy-PBPA** showed orange color emission with PL_{max} at 580 nm, whereas the emission intensity of **4BPy-PMPA** was almost quenched. Charge-transfer states are sensitive to the surrounding polarity; in polar media, the emitter dipoles are solvated, leading to the stabilization of excited states and resulting in red-shifted, broad, and quenched emission spectra.[20,21] Interestingly, even in the highly non-polar solvent, the structureless nature of the PL spectra remains intact, suggesting the strong CT nature of the singlet excited state.[22,23]

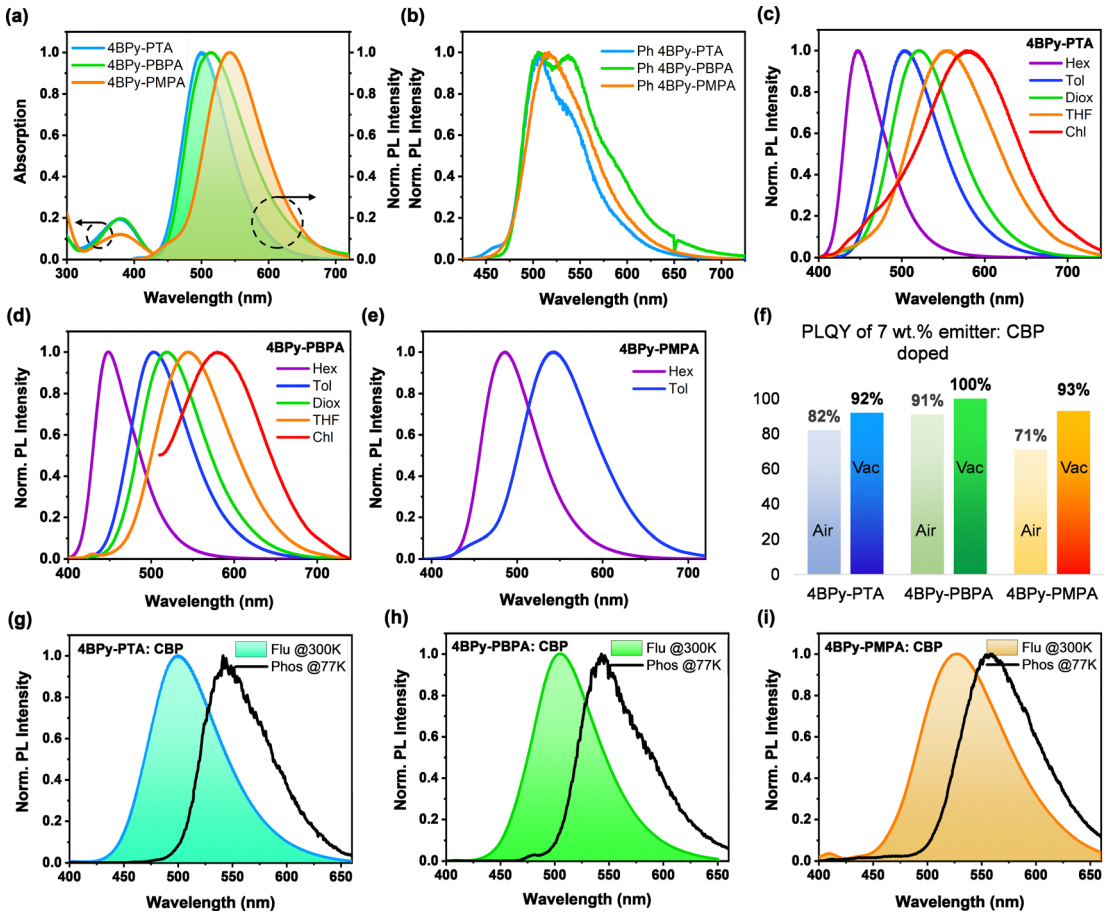

Fig. 2 Photophysical properties of the emitters; (a) UV-visible absorption in toluene and RT fluorescence; (b) LT phosphorescence in toluene; (c) solvatochromic study of **4BPy-PTA**; (d) solvatochromic study of **4BPy-PBPA**; (e) solvatochromic study of **4BPy-PMPA**; (f) PLQY of the CBP doped film; fluorescence and LT phosphorescence of the CBP doped film of (g) **4BPy-PTA**, (h) **4BPy-PBPA**, and (i) **4BPy-PMPA**.

Solid-state PL measurements were performed under 7 wt% emitter:CBP doped conditions.[24] The doped films of **4BPy-PTA** and **4BPy-PBPA** showed green emission with PL_{max} at 501 and 506 nm, respectively (Fig. 2g and h), whereas **4BPy-PMPA** showed emission in the greenish-yellow region with PL_{max} at 530 nm (Fig. 2i). It can be observed that the singlet states of the doped films and the toluene solution were isoenergetic, whereas the triplet states of the emitters were stabilized under doped conditions (Table 1 and Table S3). The stabilization of the triplet state under CBP-doped conditions was possibly due to the restriction of intramolecular bond rotation and vibration.[25] Stabilization of the triplet state resulted in increased ΔE_{ST} from 0.18, 0.14, and ~0.00 in toluene solution to 0.31, 0.28, and 0.22 eV in CBP co-doped films of **4BPy-PTA**, **4BPy-PBPA**, and **4BPy-PMPA**, respectively. The ΔE_{ST} values of these doped films are higher than the maximum theoretical energy barrier of TADF emitters ($\leq$0.2 eV). The PLQYs of the emitters under CBP co-doped conditions were measured under both ambient and inert conditions (Table 1 and Fig. 2f). Under inert conditions, the PLQY of **4BPy-PTA** was found to be 92.0%, which reduced to 82.4% when measured under ambient conditions. The triplet molecular oxygen ($^3O_2$) present in air acts as a triplet scavenger. The reduction of PLQY under ambient conditions indicates the participation of triplet excitons in the rISC process.[26,27] The PLQYs of **4BPy-PBPA** and **4BPy-PMPA** were measured to be ~100 and 93% under an inert atmosphere, which then reduced to 91 and 74%, respectively, under air conditions (Table 1 and Fig. 2f). The quantum yields of **4BPy-PTA** and **4BPy-PBPA** were significantly higher than those of their corresponding reported rigid counterparts, highlighting the crucial role of molecular flexibility in improving emission efficiency. The PLQY measurements validate the occurrence of rISC in the emitter, despite its relatively large singlet–triplet energy gap.

3.1.2. Transient PL measurements. Excited-state lifetimes were measured for the emitters under CBP co-doped conditions, showing two different lifetime components. The short fluorescence decay with lifetimes of 6.5, 5.7, and 4.6 ns for **4BPy-PTA**, **4BPy-PBPA**, and **4BPy-PMPA**, respectively, originated from the direct radiative decay from S_1 to S_0, known as prompt fluorescence (PF).[16,28] The fluorescence radiative rates (k_pR) were calculated to be on the order of 10^8 s^{-1}, which justifies the near-unity PLQY of the emitters (Fig. 3 and Table 1 and Table S7). Along with PF, the emitters also showed long fluorescence decays (delayed fluorescence/DF). Under ambient conditions, the CBP doped films of **4BPy-PTA**, **4BPy-PBPA**, and **4BPy-PMPA** exhibited weak delayed contributions with average

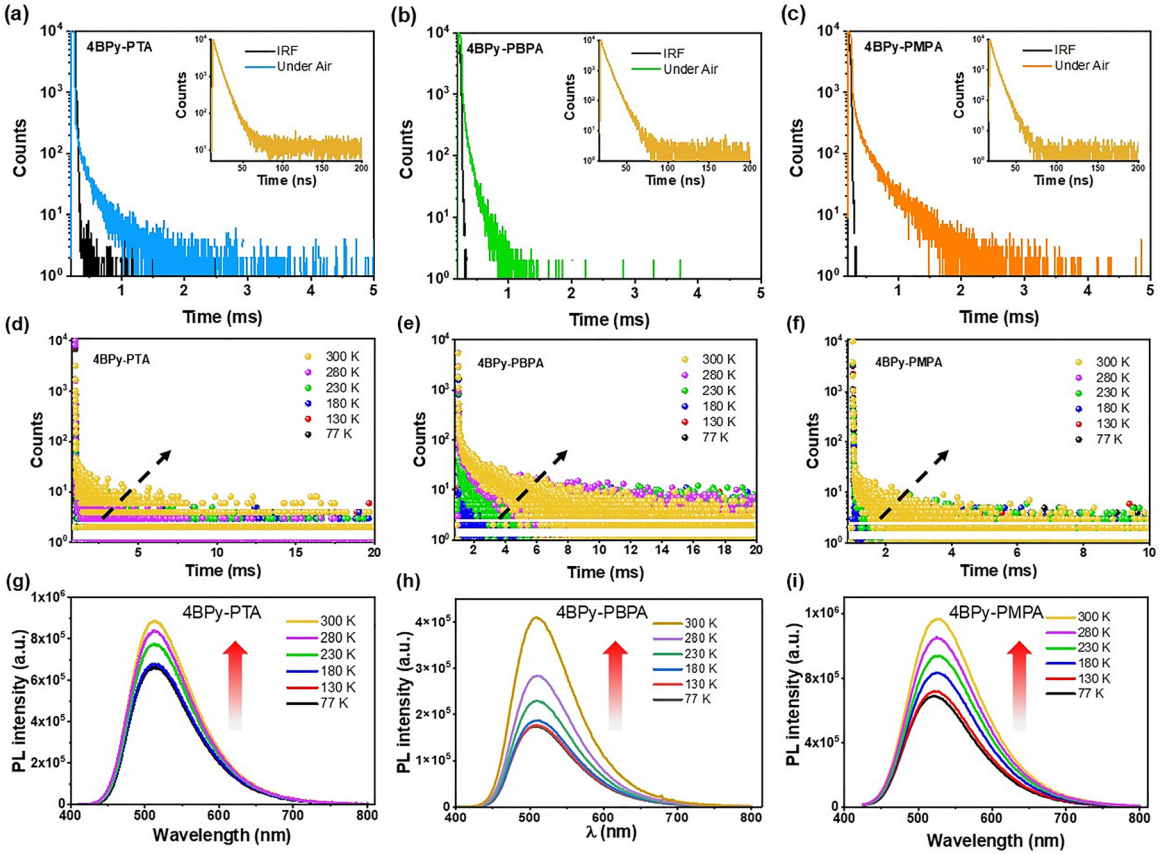

Fig. 3 Excited state lifetime measurements in 7 wt% emitter:CBP doped films; transient photoluminescence decay of (a) **4BPy-PTA**, (b) **4BPy-PBPA**, and (c) **4BPy-PMPA** measured in air (inset: prompt fluorescence component); temperature dependence of the photoluminescence (PL) characteristics of (d) **4BPy-PTA**, (e) **4BPy-PBPA**, and (f) **4BPy-PMPA**; PL spectra at different temperatures of (g) **4BPy-PTA**, (h) **4BPy-PBPA**, and (i) **4BPy-PMPA**.

lifetimes (τ_{avg}) of 13.1, 43.9, and 70.3 μs, respectively (Fig. 3a–c). However, under inert conditions, these lifetimes (τ_{avg}) were significantly enhanced to 0.86, 3.07, and 0.52 ms (Fig. 3 and Tables S4–S6). To confirm the TADF nature of the emitters, temperature-dependent transient PL measurements were performed from 77 K to 300 K and the results are shown in Fig. 3. All three emitters showed short excited state lifetimes in the range of 3–4 μs at 77 K, which gradually prolonged with increasing temperature (Fig. 3d–f). Detailed temperature-dependent lifetimes are tabulated in the SI (Tables S4–S6). This lifetime enhancement, accompanied by an increase in the PL intensity with temperature (Fig. 3g–i), unambiguously confirms the TADF characteristics of the emitters. The kinetic parameters such as the rate constants for intersystem crossing (k_{ISC}) and reverse intersystem crossing (k_{rISC}) were calculated and are summarized in Table S7.[29,30] All three emitters exhibited relatively slow k_{rISC} in the order of 10^3 s^{-1}, which is attributable to their prolonged DF lifetimes. Among the three emitters, **4BPy-PMPA** exhibits a comparatively higher k_{rISC} of 2.53×10^3 s^{-1} than **4BPy-PTA** (1.29×10^3 s^{-1}) and **4BPy-PBPA** (0.36×10^3 s^{-1}). This enhanced rISC rate in **4BPy-PMPA** is consistent with its smaller ΔE_{ST}.

3.1.3. Theoretical investigation. Unlike the reported rigid counterpart **4BPy-Cz**, **4BPy-PTA** showed a long DF lifetime and the presence of a rISC process despite having a larger S_1–T_1 energy gap, which must be linked to its excited-state nature. To further understand the electronic and excitonic properties, quantum-chemical calculations were performed.[31] The spatial distribution of natural transition orbitals (NTOs) highlights a characteristic CT nature, which was also confirmed by solvatochromic studies. Hole density/HOMOs are localized on the donor, and electron density/LUMOs concentrate over the acceptor unit (Fig. 4a and Fig. S5). The CT-dominated S_1 and T_1 states exhibit weak SOC, leading to inefficient exciton upconversion.[32] However, SOC calculations highlight the crucial role of the upper triplet excited state (T_2) in the rISC process. Theoretical calculations indicate that T_2 states possess LE character; therefore, the coupling constants between T_2 (LE) and S_1 (CT) were significantly higher than those of T_1 (CT) and S_1 (CT), indicating the central role of the T_2 state in facilitating ISC and rISC in the emitters (Fig. 4b).[32,33] Furthermore, the T_2 states of the emitters were energetically higher than the corresponding S_1 states, making the rISC process ($T_2 \rightarrow S_1$) energetically downhill and highly favorable (Fig. 4b and Table S8). Therefore, the overall triplet upconversion route would be $T_1 \rightarrow T_2 \rightarrow S_1$.

3.1.4. Electroluminescence measurements. Using the optimized 7 wt% emitter:CBP co-doped emissive layer, three OLED devices were fabricated *via* vacuum thermal deposition. The

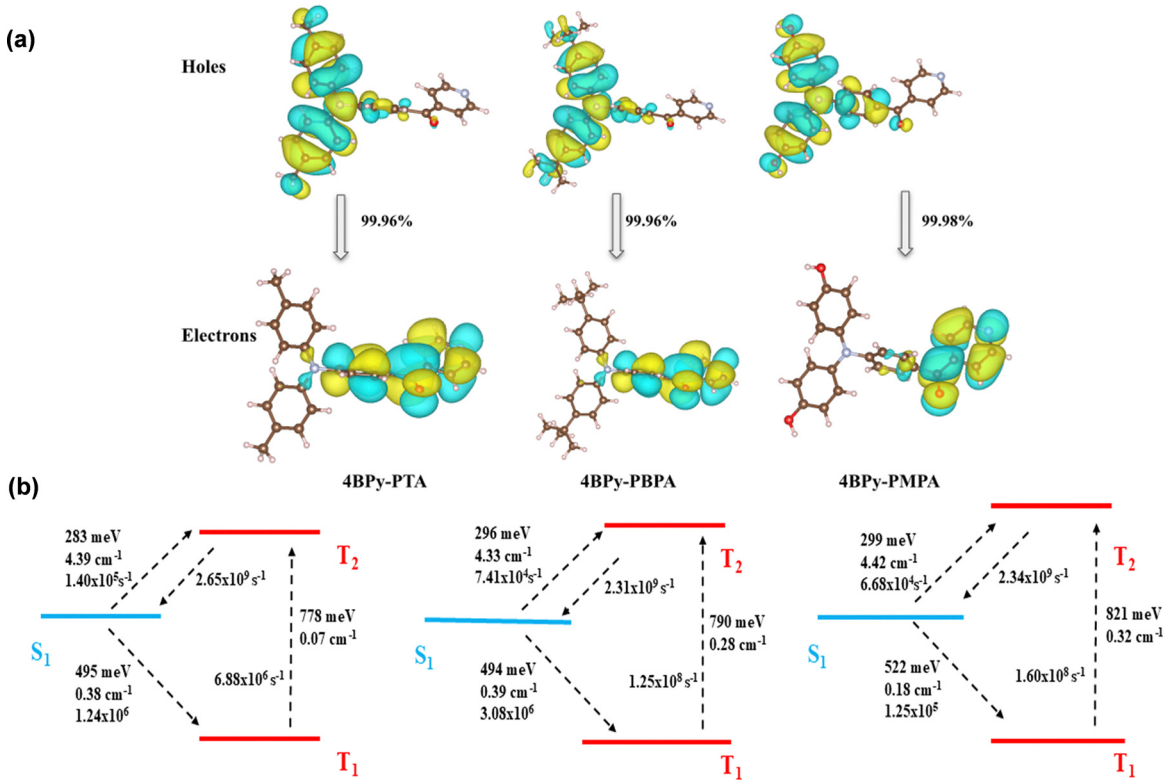

Fig. 4 (a) Natural transition orbitals (NTOs) for the $S_1 \rightarrow S_0$ transition, showing the percentage contribution from the HOMO → LUMO transition; (b) the computed electronic transitions and energy levels of **4BPy-PTA**, **4BPy-PBPA**, and **4BPy-PMPA** obtained at the B3LYP/6-31+G(d,p) level, incorporating CPCM solvent correction and dispersion correction (D3BJ) within the ORCA quantum chemistry package.

device architecture was configured as ITO/NPB (30 nm)/TAPC (20 nm)/EML (15 nm)/PPT (10 nm)/TPBi (50 nm)/Liq (2 nm)/Al (100 nm). The devices were fabricated following the standard fabrication procedure.[4] The complete device architecture and the molecular structures of the different materials used are depicted in Fig. 5a and b.

The electroluminescence maxima (EL_{max}) of **4BPy-PTA**, **4BPy-PBPA**, and **4BPy-PMPA** OLED devices were measured to be 503, 513, and 532 nm, respectively (Fig. 5 and Table 2). The EL_{max} values of the devices closely resemble the doped film PL_{max} of the emitters, confirming that the device emission originates from the EML (Tables 1 and 2). All the EL spectra of the OLEDs were structureless in appearance without having any residual peaks, indicating the proper confinement of exciton recombination within the EML (Fig. 5c–e and Fig. S6). The current density *vs.* voltage *vs.* luminance (*J–V–L*) plots of the devices are shown in Fig. S7. Among the three devices, **4BPy-PTA** showed the highest luminance maximum (L_{max}) of 10652 cd m^{-2} at 17 V (Table 2). Among the three OLEDs, the **4BPy-PBPA** device showed the highest EQE_{max} of 17.3%, followed by **4BPy-PMPA** (16.2%) and **4BPy-PTA** (6.5%). The higher EQE_{max} observed for **4BPy-PBPA** was attributed to its substantial PLQY in the doped film. Furthermore, the EQE_{max} and the calculated exciton utilization efficiency (η_{ex}) of the devices were beyond the theoretical limit of fluorescent OLEDs ($\lesssim$5%), confirming the presence of rISC and delayed fluorescence.[34,35] Interestingly, the EQE_{max} of **4BPy-PBPA** was found to be nearly double that of its reported rigid counterpart 4BPy-ptCz (9.4%), highlighting the importance of molecular flexibility in improving OLED device performance.[12]

The flexible emitters **4BPy-PTA** and **4BPy-PBPA** not only showed higher PLQYs but also exhibited better EL properties compared to their reported rigid counterparts. From the EL measurements, it can be observed that **4BPy-PBPA** and **4BPy-PMPA** show nearly similar EQE_{max}; on the other hand, despite having a higher PLQY of 92%, **4BPy-PTA** exhibited the lowest EL performance (Table 2). As discussed in the theoretical calculation, T_2 plays a crucial role in the rISC process of the emitters. Irrespective of the donor units, all three emitters showed nearly the same $T_2 \rightarrow S_1$ coupling constant (4.3–4.4 cm^{-1}) but different coupling values for $T_1 \rightarrow T_2$ (Table S8). Among the three emitters, **4BPy-PTA** exhibits the weakest $T_1 \rightarrow T_2$ coupling (0.07 cm^{-1}), rendering the overall triplet harvesting process inefficient (Fig. 4b and Table S8). Consequently, the **4BPy-PTA** molecule suffers from poor triplet exciton utilization, resulting in a lower EQE than the other two emitters. Conversely, **4BPy-PBPA** and **4BPy-PMPA**, exhibiting comparable rate constants for $T_1 \rightarrow T_2$ and $T_2 \rightarrow S_1$ transitions, witness a similar efficiency level. The internal conversion (IC) rates from the S_1 state to the ground state (S_0) for the three emitters were also calculated. **4BPy-PTA**, **4BPy-PBPA** and **4BPy-PMPA** showed IC values of 3.024×10^8, 4.322×10^7, and 5.485×10^7 s^{-1}, respectively, and this result supports the poor EL performance of **4BPy-PTA** and the efficient EL performance of **4BPy-PBPA** and **4BPy-PMPA**.

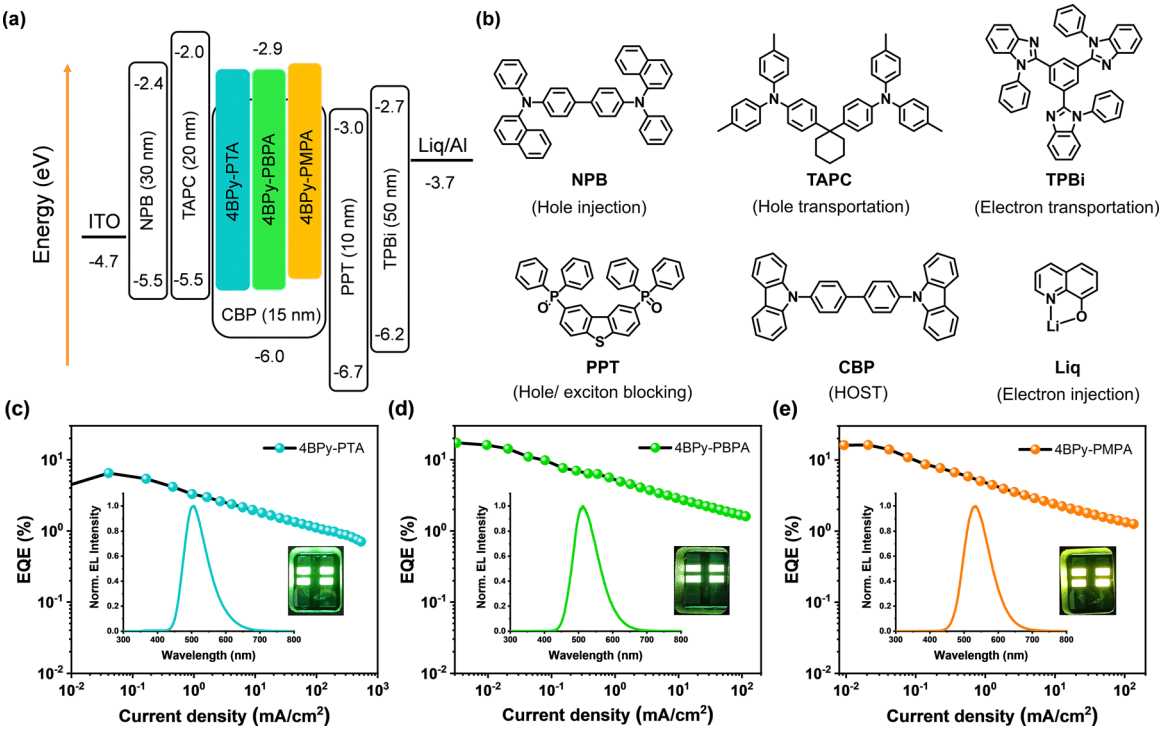

Fig. 5 EL performance of the emitters: (a) optimized OLED device architecture showing the rate of evaporation; (b) molecular structures of the materials used in the OLED device; external quantum efficiency *vs.* current density plots for the OLED devices of (c) **4BPy-PTA**, (d) **4BPy-PBPA**, and (e) **4BPy-PMPA**.

Table 2 EL performance of OLEDs

Emitter	λ_{EL}[a] (nm)	L_{max}[b] (cd m^{-2})	V_{on}[c] (V)	CE_{max}[d] (cd A^{-1})	PE_{max}[e] (lm W^{-1})	EQE_{max}[f] (%)	CIE[g] (x, y)
4BPy-PTA	504	10 652	4.5	18.1	11.4	6.5	(0.23, 0.50)
4BPy-PBPA	513	5359	3.9	50.5	39.5	17.3	(0.24, 0.51)
4BPy-PMPA	532	5633	3.5	53.5	33.6	16.2	(0.31, 0.56)

[a] Electroluminescence maxima of the OLED devices. [b] Maximum luminance of the devices. [c] Turn-on voltages of the devices at a luminance of 1 cd m^{-2}. [d] Maximum current efficiency. [e] Maximum power efficiency. [f] Maximum external quantum efficiency. [g] Commission Internationale de l'Eclairage (CIE) coordinates of the EL spectra at 7 V.

4. Conclusions

Here, we have explored the role of molecular flexibility in restoring delayed fluorescence in emitters. **4BPy-PTA**, which can be considered the flexible counterpart of the non-TADF emitter **4BPy-Cz**, starts showing delayed fluorescence properties and exhibits an EQE_{max} of 6.5%. The introduction of molecular flexibility enabled the upper triplet state to participate in the rISC process, thereby giving rise to TADF properties. A similar trend can also be observed in the other two flexible derivatives of **4BPy-PBPA** and **4BPy-PMPA**, which showed near-unity PLQY and EQE_{max} of 17.3% and 16.2%, respectively. The TADF properties of the CBP co-doped films of the emitters were confirmed through temperature-dependent PL measurements, which revealed excited state lifetimes (τ_{avg}) of 0.86 ms in **4BPy-PTA**, 3.07 ms in **4BPy-PBPA**, and 0.52 ms in **4BPy-PMPA**. Compared to its rigid counterpart (4BPy-ptCz), **4BPy-PBPA** showed a nearly twice EQE_{max} value. Strangely, despite a PLQY of 92%, **4BPy-PTA** showed the lowest EQE, mainly due to poor T_1–T_2 coupling. Both **4BPy-PBPA** and **4BPy-PMPA** showed higher T_1–T_2 coupling and lower IC than **4BPy-PTA**, which is the main reason for their better EL performance. Overall, the study highlights the crucial role of molecular flexibility in restoring the TADF properties in the system and underscores the active role of the upper triplet state in the rISC process.

Conflicts of interest

There are no conflicts of interest to declare.

Data availability

All additional characterization data, including the original spectra and detailed analyses, are provided in the supplementary information (SI). See DOI: https://doi.org/10.1039/d6tc00909c.

CCDC 2331556 and 2379582 contain the supplementary crystallographic data for this paper.[36a,b]

Acknowledgements

G. P. N. thanks Council of Scientific and Industrial Research (CSIR) India for the Senior Research Fellowship (SRF), P. R. thanks to IISc and Ministry of Human Resource Development (MHRD), India (Grant no. MoE-STARS/STARS-2/2023-0651), India-Taiwan programme of cooperation in science and technology (Grant no. 2024/IN-TW/07) and Indo German Science and Technology Centre (IGSTC/WISER 2022/RG/52/2022-23) for the financial support. The authors thank the Fund for Improvement of S&T Infrastructure (FIST) (Grant no. SR/FST/ET-II/2023/1233 (C)) for the instrumental facility at MRC, IISc Bangalore. The authors also thank INF, IISc Bangalore for the NMR facility.

References

1 E. E. Bas, P. Ulukan, A. Monari, V. Aviyente and S. Catak, *J. Phys. Chem. A*, 2022, **126**, 473–484.
2 C. H. Ryoo, J. Han, J.-H. Yang, K. Yang, I. Cho, S. Jung, S. Kim, H. Jeong, C. Lee, J. E. Kwon, I. E. Serdiuk and S. Y. Park, *Adv. Opt. Mater.*, 2022, **10**, 2201622.
3 Y. Song, B. Li, S. Liu, M. Qin, Y. Gao, K. Zhang, L. Lin, C.-K. Wang and J. Fan, *J. Mater. Chem. C*, 2022, **10**, 4723–4736.
4 G. P. Nanda, R. Suraksha, B. Sk, T. Viswanathan and P. Rajamalli, *J. Mater. Chem. C*, 2025, **13**, 14953–14961.
5 H.-T. Feng, J. Zeng, P.-A. Yin, X.-D. Wang, Q. Peng, Z. Zhao, J. W. Y. Lam and B. Z. Tang, *Nat. Commun.*, 2020, **11**, 2617.
6 T. Matulaitis, P. Imbrasas, N. A. Kukhta, P. Baronas, T. Bučiūnas, D. Banevičius, K. Kazlauskas, J. V. Gražulevičius and S. Juršėnas, *J. Phys. Chem. C*, 2017, **121**, 23618–23625.
7 F.-M. Xie, J.-X. Zhou, Y.-Q. Li and J.-X. Tang, *J. Mater. Chem. C*, 2020, **8**, 9476–9494.
8 P. Rajamalli, V. Thangaraji, N. Senthilkumar, C.-C. Ren-Wu, H.-W. Lin and C.-H. Cheng, *J. Mater. Chem. C*, 2017, **5**, 2919–2926.
9 T. Kalab, A. T. Gogoulis, B. O. Patrick and Z. M. Hudson, *Chem. – Eur. J.*, 2025, **31**, e02760.
10 S. Dey, A. K. Pal, M. Upadhyay, A. Datta and D. Ray, *J. Phys. Chem. B*, 2023, **127**, 9833–9840.
11 H. Ma, Q. Peng, Z. An, W. Huang and Z. Shuai, *J. Am. Chem. Soc.*, 2019, **141**, 1010–1015.
12 P. Rajamalli, N. Senthilkumar, P. Gandeepan, C.-C. Ren-Wu, H.-W. Lin and C.-H. Cheng, *ACS Appl. Mater. Interfaces*, 2016, **8**, 27026–27034.
13 G. P. Nanda, R. Suraksha and P. Rajamalli, *ACS Mater. Au*, 2024, **4**, 604–611.
14 P. A. Forero-Cortés and A. M. Haydl, *Org. Process Res. Dev.*, 2019, **23**, 1478–1483.
15 S. Wu, W. Li, K. Yoshida, D. Hall, S. Madayanad Suresh, T. Sayner, J. Gong, D. Beljonne, Y. Olivier, I. D. W. Samuel and E. Zysman-Colman, *ACS Appl. Mater. Interfaces*, 2022, **14**, 22341–22352.
16 H. Uoyama, K. Goushi, K. Shizu, H. Nomura and C. Adachi, *Nature*, 2012, **492**, 234–238.
17 Y. Tao, K. Yuan, T. Chen, P. Xu, H. Li, R. Chen, C. Zheng, L. Zhang and W. Huang, *Adv. Mater.*, 2014, **26**, 7931–7958.
18 P. Rajamalli, N. Senthilkumar, P. Gandeepan, C.-Z. Ren-Wu, H.-W. Lin and C.-H. Cheng, *J. Mater. Chem. C*, 2016, **4**, 900–904.
19 A. K. Mazumdar, G. P. Nanda, N. Yadav, U. Deori, U. Acharyya, B. Sk and P. Rajamalli, *Beilstein J. Org. Chem.*, 2022, **18**, 1177–1187.
20 S. Nigam and S. Rutan, *Appl. Spectrosc.*, 2001, **55**, 362A–370A.
21 R. Kumari, A. Varghese, L. George and Y. N. Sudhakar, *RSC Adv.*, 2017, **7**, 24204–24214.
22 W. Z. Yuan, X. Bin, G. Chen, Z. He, J. Liu, H. Ma, Q. Peng, B. Wei, Y. Gong, Y. Lu, G. He and Y. Zhang, *Adv. Opt. Mater.*, 2017, **5**, 1700466.
23 C. Fu, S. Luo, Z. Li, X. Ai, Z. Pang, C. Li, K. Chen, L. Zhou, F. Li, Y. Huang and Z. Lu, *Chem. Commun.*, 2019, **55**, 6317–6320.
24 Y. Q. Zhang, G. Y. Zhong and X. A. Cao, *J. Appl. Phys.*, 2010, **108**, 083107.
25 A. D. Sontakke, J.-M. Mouesca, V. Castaing, A. Ferrier, M. Salaün, I. Gautier-Luneau, V. Maurel, A. Ibanez and B. Viana, *Phys. Chem. Chem. Phys.*, 2018, **20**, 23294–23300.
26 M. A. Filatov, S. Baluschev and K. Landfester, *Chem. Soc. Rev.*, 2016, **45**, 4668–4689.
27 C. Schweitzer, Z. Mehrdad, F. Shafii and R. Schmidt, *Phys. Chem. Chem. Phys.*, 2001, **3**, 3095–3101.
28 U. Deori, E. Ravindran, G. P. Nanda, S. G. Ramanath, U. Acharya, P. Gandeepan and P. Rajamalli, *Chem. – Asian J.*, 2023, **18**, e202300352.
29 G. P. Nanda, S. Chand, S. Rajamanickam and P. Rajamalli, *Chem. Commun.*, 2024, **60**, 9234–9237.
30 N. Yadav, U. Deori, E. Ravindran, B. Sk and P. Rajamalli, *J. Mater. Chem. C*, 2023, **11**, 16368–16376.
31 F. Neese, *WIREs Comput. Mol. Sci.*, 2012, **2**, 73–78.
32 M. A. El-Sayed, *J. Chem. Phys.*, 1963, **38**, 2834–2838.
33 M. Baba, *J. Phys. Chem. A*, 2011, **115**, 9514–9519.
34 D. Y. Kondakov, *Philos. Trans. R. Soc., A*, 2015, **373**, 20140321.
35 B. Sk, V. Thangaraji, N. Yadav, G. P. Nanda, S. Das, P. Gandeepan, E. Zysman-Colman and P. Rajamalli, *J. Mater. Chem. C*, 2021, **9**, 15583–15590.
36 (*a*) CCDC 2331556: Experimental Crystal Structure Determination, 2026, DOI: 10.5517/ccdc.csd.cc2j85hh; (*b*) CCDC 2379582: Experimental Crystal Structure Determination, 2026, DOI: 10.5517/ccdc.csd.cc2kw4qb.

